Prism Dose Computation Methods *

Ira J. Kalet, Jonathan P. Jacky,
Paul Cho, Mark A. Martin

Technical Report 93-09-01

Radiation Oncology Department RC-08
University of Washington
Seattle, WA 98195

April 11, 1994

*This work was supported in part by NIH grant LM04174 from the National Library of Medicine, NIH contract CM97566 from the National Cancer Institute, and a grant from General Electric Medical Systems, Milwaukee, Wisconsin.

©1993 by Ira J. Kalet, Jonathan P. Jacky, Paul Cho and Mark A. Martin. This work may not be copied or reproduced in whole or part for any commercial purpose. Permission to photocopy in whole or part without payment of fee is granted for nonprofit educational and research purposes provided that all such copies include the following notice: a notice that such copying is by permission of the authors; an acknowledgement of the authors of the work; and all applicable portions of this copyright notice. All rights reserved.

Contents

1 Photon and neutron beams **4**

1.1 Rectangular collimators 4

1.1.1 Calibration distance 6

1.1.2 Absolute dose calibration 6

1.1.3 Output vs. field size 7

1.1.4 Tissue-phantom ratio 7

1.1.5 Off-center ratios 8

1.1.6 Inhomogeneity and obliquity correction 9

1.1.7 Wedges 9

1.1.8 Blocks 9

1.2 Multileaf collimators 11

1.2.1 Introduction 11

1.2.2 Output factor 12

1.2.3 Equivalent square field size 14

1.2.4 Tissue-phantom ratio 14

1.2.5 Off-center ratio 15

2 Electrons **15**

2.1 Theory 15

2.2 Numerical Implementation 16

2.3 Measurements required by the Electron Beam Calculation 18

3 Arc therapy **19**

4 Dose conversion algorithms **19**

4.1 Depth Dose to TPR 19

4.2 TPR to SPR 20

5 Line and point sources **21**

This document describes the methods that the Prism system uses to calculate doses and dose rates for the various types of treatment plans. It also includes information about deriving some of the required data from other related data.

1 Photon and neutron beams

This section describes how dose calculations are done for megavoltage photons and fast neutrons. The dose computations are based on tissue phantom ratios, a modification of the tissue-air ratio concept. The rationale for these calculations is outlined in [1]; a more thorough review is offered by [2].

Two kinds of collimation systems are modelled, including:

- Rectangular collimator systems, in which either or both sets of collimator jaws have the possibility that each jaw can move independently. This type represents symmetric, combination, and variable jaw collimators. However, overcentering of combination or variable jaw collimators is not supported.
- Multileaf collimator systems, in which the collimator consists of a large number of independently moveable thin vanes, that can be used to form a highly irregular field shape.

The model for rectangular jaw systems accomodates the addition of shielding blocks, but the multileaf model does not (the multileaf collimator design obviates the need for blocking, generally).

The dose computation model requires that the absolute dose calibration be measured at the isocenter, and all other measurements that refer to a reference point or calibration point are made using the isocenter as that point.

Each type of collimator system is handled somewhat differently. In the following sections they are described in detail.

1.1 Rectangular collimators

The dose D at a point P inside the patient (see figure 1) due to a single fixed external photon or neutron beam source with a rectangular collimator is calculated by the formula

$$D = \left(\frac{F}{F+m}\right)^2 \cdot D_{cal} \cdot O(w_c) \cdot [TPR(w_d, d) \cdot OCR(w_1, d, \frac{2x}{w_1}) \cdot OCR(w_2, d, \frac{2y}{w_2}) - B] \cdot I \cdot W \quad (1)$$

where D is dose per machine unit at point P within the patient.

The input variables are defined as follows:

- F is the distance from the nominal source to the isocenter
- m is the distance from the isocenter to the point at which the central axis intersects the perpendicular line which passes through point P

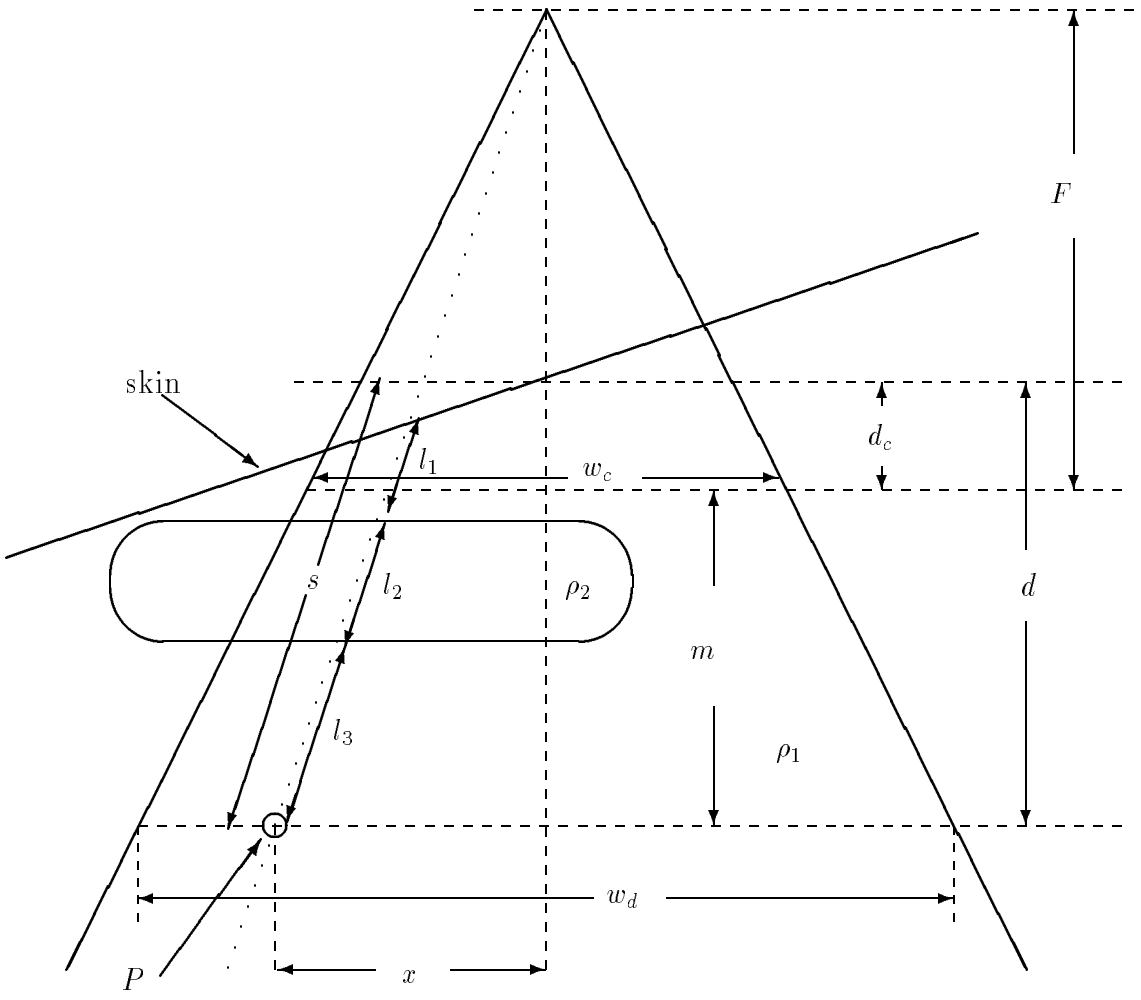

Figure 1: The basic geometry for external beam dose computation

- D_{cal} is the absolute dose calibration at the calibration point (isocenter)
- w_c is the field size at the calibration distance F from the source
- $O(w_c)$ is the relative output for the indicated field size at the calibration point
- d is the depth of the point P below the surface, measured along the central axis of the beam from the point of intersection between the central axis and the contour to the level of the point, but on the central axis
- w_d is the equivalent square field size at depth d
- TPR is the tissue-phantom ratio for the indicated field size and depth
- OCR is the off-center ratio (w_1 and w_2 are full-field dimensions at depth d)
- x, y are the lateral distances from beam centerline to point P

- B is the block factor, calculated by sector integration.
- I is a correction for patient's curvature and tissue inhomogeneity
- W is a wedge attenuation correction factor

We now describe each of these terms in more detail.

1.1.1 Calibration distance

F is a constant for each photon or neutron therapy machine, the distance from nominal source to isocenter, and is determined by the machine's design: for example, 80 cm for most cobalt machines, or 100 cm for most linear accelerators. For the CNTS neutron gantry, F is 150 cm.

1.1.2 Absolute dose calibration

D_{cal} is the dose per machine unit measured at reference depth d_c within a water phantom, such that the detector is distance F from the nominal source, and the field size at that distance is 10×10 cm. (see figure 2). Note that the phantom's surface is distance $(F - d_c)$ from the source. D is expressed in rads per machine unit. For cobalt, the machine unit is usually one minute, and for accelerators, it is one monitor unit. The calibration is made with the ion chamber at the isocenter. Most accelerators are adjusted so that $D_{cal} = 1.0$.

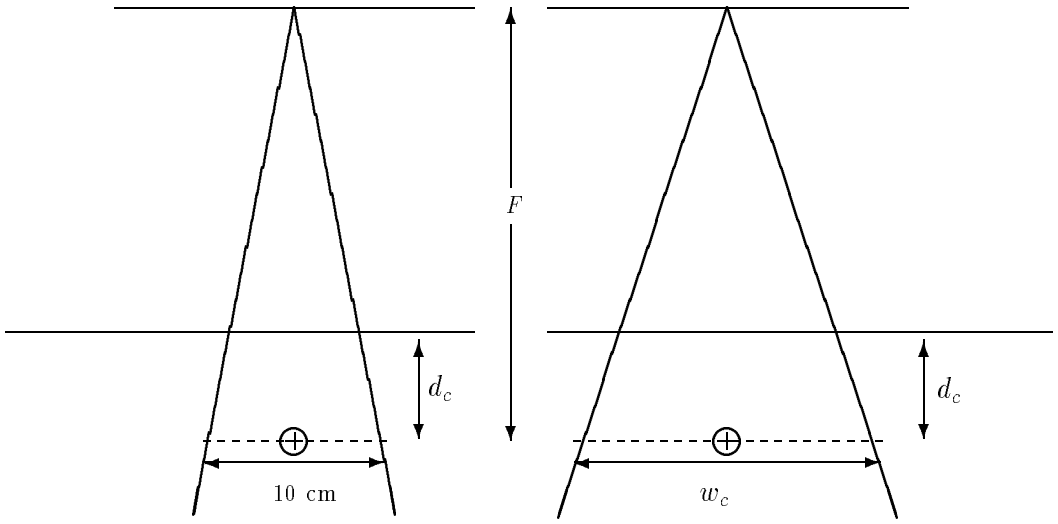

Figure 2: Calibration geometry

1.1.3 Output vs. field size

$O(w_c)$ is dose per machine unit at equivalent square field size w_c at calibration distance F from the source, relative to the dose per machine unit measured under the same conditions but in a 10×10 field. This value is obtained from tabulated values of doses measured in the same way as the absolute calibration (figure 2), but at a series of different collimator settings specified by the physicist. If w_c differs from any field size for which data have been tabulated, $O(w_c)$ is obtained by linear interpolation between the nearest tabulated values. The equivalent square field size is $4A/P$ using area and perimeter values at the isocenter.

1.1.4 Tissue-phantom ratio

$TPR(d, w_d)$ is the ratio of the dose at a point A at depth d inside the phantom to the dose at a point B at reference depth d_c inside the phantom,

$$TPR(d, w_d) = \frac{dose@A}{dose@B} = \frac{D(d, w_d, F)}{D(d_c, w_d, F)} \tag{2}$$

where points A and B are both at a distance F from the source and are both on the central axis of fields of size w_d (figure 3).

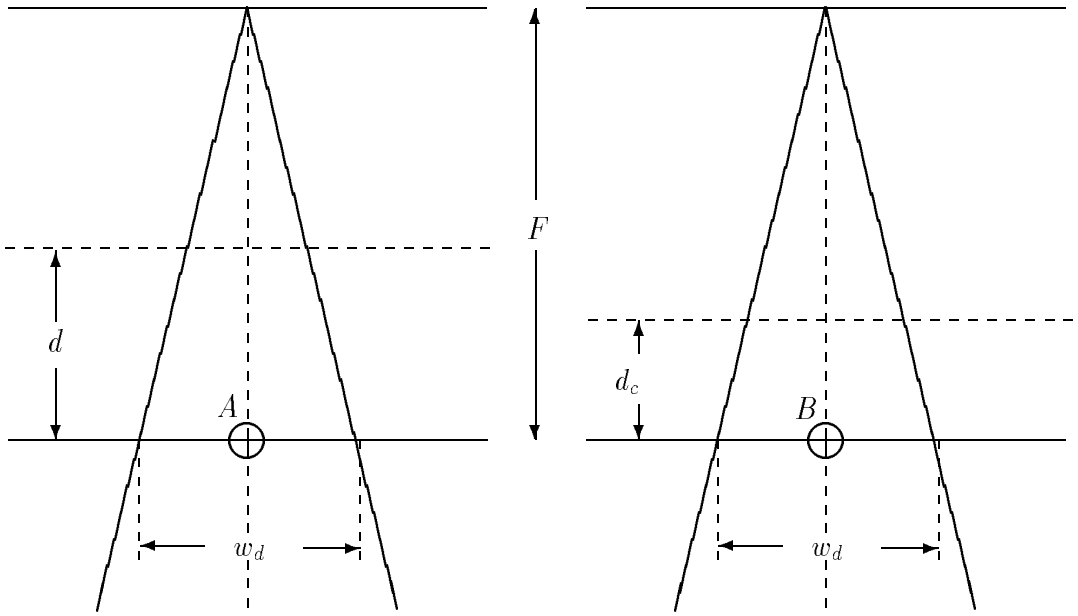

Figure 3: TPR measurement geometry

For rectangular fields, the TPR used in the dose computation formula corresponds to the "equivalent square field". That is, the field size argument w_d is set equal to $4A/P$ where A and P are the area and perimeter, respectively, of the rectangular field at depth d.

1.1.5 Off-center ratios

The OCR factors in equation 1 are interpolated from a table of measured OCR factors. The OCR factor for each direction is based on a field size corresponding to the jaw opening on the same side as the point. Note that overcentered jaw positions are not supported. The values w_1 and w_2 are computed from the collimator settings (i.e., the field dimensions at the isocenter), by multiplying by the divergence factor, $F/(F+m)$ so we assume the same divergence for geometric field size as for variation of dose rate with distance from the source. w_1 and w_2 are each twice the corresponding jaw setting on the same side of the isocenter as the point of dose calculation. Then, x and y are the absolute values of the corresponding point coordinates. Collimator jaw settings increase as the jaws open away from the isocenter.

OCR's are obtained in a water phantom at several collimator settings specified by the physicist. The distance from the source to the phantom surface must be the same $(F - d_c)$ as in other series of measurements. For each collimator setting, OCR's must be measured at the same series of depths. At each depth, OCR's are measured at the same series of beam width ratios x_d/w_d, which are specified by the physicist, where x_d is twice the lateral distance from the center of the field and w_d is the field size at that depth (figure 4).

OCR's may be measured at equally spaced x_d/w_d; alternatively, you may choose x_d/w_d values which are more closely spaced near the beam edge. OCR's are normalized to the dose on the central axis of the beam at the corresponding depth.

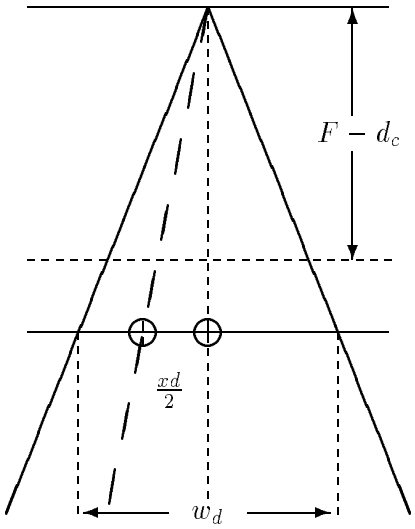

Figure 4: OCR measurement geometry

1.1.6 Inhomogeneity and obliquity correction

The effects of the patient's curvature and tissue inhomogeneity are corrected for by the factor I in the dose computation formula. I is a ratio of tissue phantom ratios

$$I = \frac{TPR(w_d, l)}{TPR(w_d, s)} \tag{3}$$

where the depth arguments are defined as follows (see figure 1):

- s is the slant height to the surface which is perpendicular to the central axis of the beam and passes through the point of intersection between the central axis and the contour,
- l is the tissue equivalent path length, which is in turn defined by $l = \sum_i l_i \cdot p_i$ where l_i is the path length through the *i-th* region and p_i is the effective density of the *i-th* region.

For example, in figure 1 we obtain

$$l = l_1 \cdot p_1 + l_2 \cdot p_2 + l_3 \cdot p_1 \tag{4}$$

where p_1 appears in the third term because that part of the path is now back in region 1.

1.1.7 Wedges

The attenuation through wedges is corrected for by the factor W in equation 1, which is determined by interpolating a wedge attenuation profile that is entered as part of the beam data for each machine. A single profile at a representative depth (e.g., 10 cm) may be used for all depths, or you may enter a series of wedge profiles at up to 5 depths. Therefore you do not provide measured data for a series of "wedged fields" of different field sizes.

Measured wedge attenuation profiles are taken with the collimator(s) open to the largest field size you would use with a wedge in place, along a line perpendicular to the central axis, through the isocenter. The wedge factor for each position along this line is the ratio of the dose measured with the wedge in place to the dose without the wedge (for the same number of monitor units).

1.1.8 Blocks

Blocks are handled by doing a separate scatter integration of the block area only, as a negatively weighted field, which is then combined with the open field calculation to give a composite dose. This accounts for the effect of direct attenuation of the block and also the effect of missing scatter from the region under the block. Any number of blocks of any irregular outlines can be handled for each field, but no block's outline may overlap or intersect any other block's outline, in that single field. The outline may be drawn either clockwise or counterclockwise, and must not intersect itself. It does not need to be convex. C-shaped outlines are permitted.

The block factor B in equation 1 is computed by

$$B = \sum_{blocks} (1 - t_{block})(TPR(0, d) \cdot PRIM + SCAT) \tag{5}$$

where each block is treated as a separate field outline, and is weighted by a factor $(1-t)$, t being the transmission factor for *each* block. The primary ($PRIM$) and scatter ($SCAT$) components are computed by methods similar to the IRREG program [**?**]. The block outlines are clipped to the collimator openings, so in effect we are computing the amount by which the block reduces the dose from the open field. The total block factor is the sum of the individual ones.

$$PRIM = OCR\left(w_n, d, \frac{w_n - 2r_{min}}{w_n}\right) \tag{6}$$

$$SCAT = \sum_{j=1}^{a}\left[\frac{\text{sign}_j \cdot \theta_j}{2\pi n}\sum_{i=1}^{n} SPR(d, r_i)\right] \tag{7}$$

where w_n is the field width for the nearest collimator (it should be w_1 or w_2, whichever is nearest). The minimum radial distance, r_{min}, is the distance to the nearest point on the block edge; it is positive if the point is inside the block shadow, and negative if the point is outside the block shadow. In the scatter sum, a is the number of sides in the polygon defining the block shape, and n is the number of sectors in each of the sides.

Each side of the block polygon is divided up into a series of sectors. For each side the sign associated with the side is the sign of the z component of the vector cross product, $\vec{V}_1 \times \vec{V}$. The vector $\vec{V}_1$ goes from the point of calculation to the beginning of the side, and the vector $\vec{V}$ is the side itself. The angle θ_j is the angle subtended by the side j at the point of calculation. It is computed from the vector cross product $\vec{V}_1 \times \vec{V}_2$ and the dot product $\vec{V}_1 \circ \vec{V}_2$. The vector $\vec{V}_2$ goes from the point of calculation to the end of the polygon side.

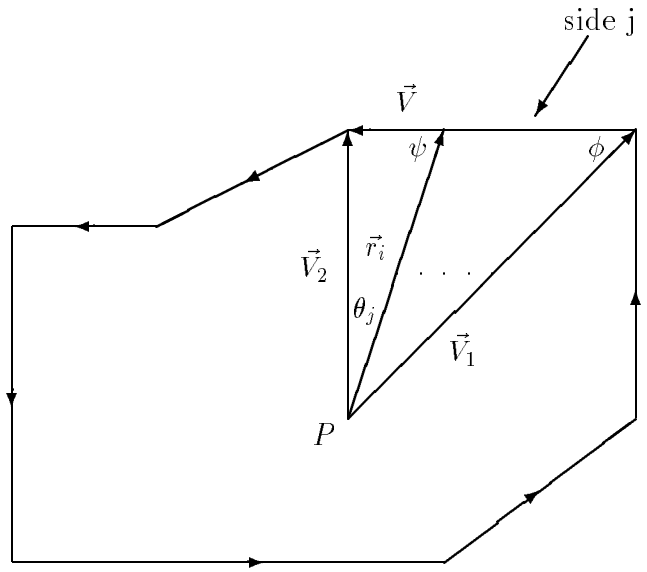

Figure 5: Sector scatter summation

Since

$$|\vec{V}_1 \times \vec{V}_2| = |\vec{V}_1| \cdot |\vec{V}_2| \cdot \sin\theta \tag{8}$$

$$\vec{V}_1 \circ \vec{V}_2 = |\vec{V}_1| \cdot |\vec{V}_2| \cdot \cos\theta \tag{9}$$

we can compute θ from

$$\theta = \arctan\left(\frac{|\vec{V}_1 \times \vec{V}_2|}{\vec{V}_1 \circ \vec{V}_2}\right) \tag{10}$$

and in our system, θ is always taken as a positive quantity between 0 and π. The arctan functon always returns a value between 0 and $\pi/2$ so the sign of the dot product is used to determine which quadrant (first or second) the angle is in. The contribution of the side to the sum may be positive or negative as determined by the sign of the cross product. Overall, the calculation is symmetric with respect to whether the outline goes clockwise or counter clockwise, and at the end, the absolute values of primary and scatter are used in calculating the block factor.

The SPR value used for each sector is determined from the point depth and a computed sector radius. The point depth is the depth on the central axis corresponding to the point of calculation. The sector radius is computed by dividing up the side into sectors of no larger than 10^o. The sector radius is

$$r_{sector} = \frac{|\vec{V}_1 \times \vec{V}|}{|\vec{V}| \sin\psi} \tag{11}$$

where ψ is the sector angle. This angle ranges from the angle ϕ between $\vec{V}_1$ and $\vec{V}$, and $\phi + \theta$. The angle ϕ may be determined in the same way as θ from

$$\phi = \arctan\left(\frac{|\vec{V}_1 \times \vec{V}|}{\vec{V}_1 \circ \vec{V}}\right) \tag{12}$$

except that ϕ is the supplemental angle, inside the triangle formed by $\vec{V}_1$, $\vec{V}_2$ and $\vec{V}$. This arises because $\vec{V}_1$ and $\vec{V}$ are head to tail rather than tail to tail as are $\vec{V}_1$ and $\vec{V}_2$.

The primary (for the irregularly shaped field defined by the block) is set equal to the scatter at points that are more than a distance 0.1 times the collimator half-width outside the block. At other points the primary is calculated using equation 6.

1.2 Multileaf collimators

1.2.1 Introduction

The multileaf model is quite similar to our longstanding model for conventional collimators, but is adapted to accommodate any (potentially quite irregular) field shape that might be created by a leaf collimator.

The multileaf model is the same for both neutrons and photons. Any differences between dose distributions must derive from differences in tables of measured beam data and other empirically determined constants, not from different calculations.

The multileaf model does not accomodate the addition of shielding blocks (the multileaf collimator design obviates the need for blocking, generally).

Here is the formula for our conventional collimator model, quoted from equation 1. The dose D to a point P (see Fig. 1) is:

$$D = \left(\frac{F}{F+m}\right)^2 \cdot D_{cal} \cdot O(w_c) \cdot [TPR(w_d, d) \cdot OCR(w_1, d, \frac{2x}{w_1}) \cdot OCR(w_2, d, \frac{2y}{w_2}) - B] \cdot I \cdot W \quad (13)$$

The multileaf collimator model is:

$$D = \left(\frac{F}{F+m}\right)^2 \cdot D_{cal} \cdot O_p(w_p) \cdot TPR(w_b, d) \cdot OCR(w_b, d, \frac{x_{min}}{w_b}) \cdot I \cdot W \quad (14)$$

The variables that differ from the rectangular collimator model are:

- $O_p(w_p)$ is the relative output calculated for the portal shape
- w_b is the equivalent square field size calculated for the portal shape at the calibration distance
- $TPR(w_b, d)$ is the tissue phantom ratio calculated for the portal shape and the depth d.
- $OCR(w_b, d, \frac{x_{min}}{w_b})$ is the off-center ratio calculated for the portal shape, the depth d, and the point P.

Each of these new items is described in greater detail in the following sections.

1.2.2 Output factor

The calculation of a relative output factor $O_p(w_p)$ for the (possibly quite irregular) portal shape is the biggest difference from the calculation for conventionally collimated fields.

The calculated relative output factor $O_p(w_p)$ will be the same as the output factor for the square field with side w_p. However, we do *not* first calculate w_p and then look up the output factor for that square field size. Instead, we calculate the output factor $O_p(w_p)$ directly from the irregular portal shape.

Our calculation of $O_p(w_p)$ is based on the idea that each area element in the field portal contributes an increment to the total output factor. The increment contributed by each element is a function of the area of the element, and of the position of the element in the field. In other words, $O_p(w_p)$ is obtained by integrating a weighting function over the portal shape.

The problem, then, is to choose a weighting function that results in a calculated $O_p(w_p)$ that agrees closely with measured output factors in clinically useful field shapes. In particular, it must agree very closely with the tables of measured square field output factors that are entered in the treatment planning beam database.

When output factors for square fields are plotted as a function of field size, the curve is concave toward the horizontal axis; adding area to a small field causes a bigger change in output factor than adding the same area to a large field. Therefore, the weighting function must be larger near the central axis than at the periphery.

We calculate $O_p(w_p)$ by adding together two components. The first component, called the *area component*, is $O_a(w_a)$. The area component is calculated from the area a of the field portal at the calibration distance, determined by a geometric planimetry calculation. The effective field size is simply the square root of this area: $w_a = \sqrt{a}$. Then the area component $O_a(w_a)$ is found by looking up the output factor for w_a in the table of measured square field output factors.

The second component, called the *weighted component*, is $O_w(c_p)$. This weighted component is calculated directly from the contour that defines the portal shape at the calibration distance, c_p; there is no calculation of any single equivalent square field size. Instead, the program performs a Clarkson-like sector integration, similar to that described in Section 1.1.8, Figure 5. The field is divided into a large number of radial sectors by drawing radii from the central axis to the edge of the portal. For each sector, we look up the output factor for the square field with the same average radius. Then we add all these contributions together, weighting the contribution from each sector by the angle subtended by that sector.

There is an additional complication in the calculation of the weighted component of the output factor. The sector integration tends to weight the middle of the field much too heavily — almost all the output factor ends up being contributed by the few square cm in the middle. Thus, the output factor estimated for a midline blocked or half-beam blocked field is much too small. To fix this, we say that for "sufficiently large" fields there is a minimum output factor below which the output factor cannot fall, even if there is blocking near the field center. We characterize this minimum output factor by the diameter of the (unblocked) circular field that has that output factor. We call this number the *virtual source diameter*. Additional field area outside the disk defined by this diameter contributes additional output factor. Dose calculations for fields with no blocking that intrudes inside the disk should be unaffected by the choice of this parameter.

The combined output factor is formed from the weighted sum of the two components:

$$O_p(w_p) = (1 - k) \cdot O_a(w_a) + k \cdot O_w(c_p) \tag{15}$$

The constant k, the weighting of the weighted component in the combined output factor, is called the *collimator constant*. Both components of the output factor are defined so they agree very closely with the measured square field output factors. Therefore, their weighted sum will also agree closely for any choice of k from 0.0 to 1.0.

The virtual source diameter and the collimator constant are two adjustable parameters that the physicist should choose to give good agreement to measured dose distributions created by fields with blocking near the central axis. The physicist can set and examine the values of both parameters using a beam data utility. A different pair of values is stored for each beam. As a starting point, it works reasonably well to set both parameters to 0.0. At this writing, we are using these values:

Beam	Collim. const.	Source diam.
Neutron	0.03	0.0
SL20 6X	0.01	0.3
SL20 18X	0.00	n/a

These values were chosen "by eye," not by applying any numerical optimization method.

We find that our method gives acceptable clinical accuracy for the two SL20 photon beams, but not for the neutron beam. In particular, it overestimates the output factor for elongated neutron fields. Making the collimator constant larger gives better agreement for the elongated fields, but then it underestimates the output factor for midline blocked and half-beam-blocked neutron fields.

This method for calculating the output factor is admittedly rather ad-hoc. It was chosen because it was easy to implement by modifying code that we already had. It might be possible to achieve better results by doing a straightforward numerical integration using some parameterized analytical expression as the weighting function, with parameter values chosen by some numerical optimization method, instead of "by eye."

To calculate $O_p(w_p)$ we never actually compute the equivalent square field size w_p; we calculate the output factor directly from the irregular portal shape. Once we have our output factor, we can look up the square field size w_p which has that same output factor. We provide this w_p solely for the benefit of the dosimetrists and physicists who review the treatment plan. They can determine whether the w_p calculated by the program is consistent with their own judgment of the square field size that is equivalent to the actual field shape. They may use w_p to perform a hand calculation that should agree closely with the doses calculated by the program.

1.2.3 Equivalent square field size

The equivalent square field size used to look up the tissue phantom ratio (TPR) and the off-center ratio (OCR) is w_b. It is different from w_p, the equivalent square for the output factor, and is calculated by a much simpler method.

To calculate w_b, we simply find the smallest rectangle with sides parallel to the axes of the collimator coordinate system that completely encloses the leaf collimated portal shape at the calibration distance. The value of w_b is the side of the equivalent square to this rectangle, calcuated by $4A/P$.

The enclosing rectangle for this calculation is always oriented so that two of its sides are parallel to the direction of leaf motion. Therefore, if the portal shape is a square rotated 45 degrees to a "diamond" orientation (with its points on the collimator coordinate system axes, and its diagonal sides formed by stepped leaves), the calculated w_b will be considerably larger than the side of the portal.

1.2.4 Tissue-phantom ratio

$TPR(w_b, d)$ is the tissue phantom ratio calculated for the portal shape and the depth d. It is calculated in exactly the same way as for conventional collimators, except it uses w_b (described above) instead of w_d. For each point, the field width used to look up the TPR is the field width *at the depth of the point*, that is, w_b scaled by the magnification factor from the depth of the isocenter to the depth of the point of interest.

1.2.5 Off-center ratio

For leaf collimators, the off-axis effect is accounted for by only a single OCR, not a product of two OCR's as in rectangular fields.

$OCR(w_b, d, \frac{x_{min}}{w_b})$ is the off-center ratio calculated for the portal shape, the depth d, and the point P. It is calculated in much the same way as an OCR for conventional collimators, except it uses w_b (described above) for the field width instead of a width w_1 or length w_2.

In order to calculate the fan line ratio, the program finds r_{min}, the shortest distance from the point of calculation to any side of the field portal, all scaled to the calibration distance. Then it calculates $x_{min} = w_b - 2 \cdot r_{min}$. The fractional half-beamwidth used to look up the OCR is $\frac{x_{min}}{w_b}$.

The calculation only uses a single OCR profile that tabulates ratios from the central axis outward in one direction, even though the profile shape might differ depending on whether the point of interest lies near a field edge defined by the ends of the leaves or by their sides (or by a collimator diaphragm). It is up to the physics staff to determine how this single profile should be formed from all the available profile data (for example, whether profiles are averaged or a single measured profile is chosen).

2 Electrons

The electron beam dose calculation is a pencil beam model that can compute dose to arbitrary points in a 3-dimensional volume delineated by contours as for photons and neutrons. It can handle arbitrary apertures and inhomogeneity corrections.

2.1 Theory

The pencil-beam algorithm was originally proposed by Hogstrom et al [3]. The method is based on Eyges' solution to Fermi's transfer equation [4] which simplifies the electron transport by assuming that the electrons undergo only multiple, small-angle, elastic scattering. In this case, the lateral fluence distribution of the pencil-beam may be approximated as Gaussian.

The pencil-beam formulation relies on the fact that, within a few percent, the total electron fluence has the same depth dependence as the absorbed dose. It follows that by summing the fluence contribution of each pencil beam to a point of interest the dose can be estimated.

The dose to a point (x, y, z) from a set of pencil-beams at depth z is given by:

$$D(x,y,z) = \int_{-\infty}^{\infty}\int_{-\infty}^{\infty} \frac{1}{2\pi\sigma_{MCS}^2} \exp\left(-\frac{(x-x')^2+(y-y')^2}{2\sigma_{MCS}^2}\right) S_{air}(x',y',z) F2D(D_{eff}) \left(\frac{SAD+D_{eff}}{SAD-z}\right)^2 dx'dy' \quad (16)$$

Here, (x', y') is the coordinate of the pencil-beam axis at depth z, D_{eff} is the density-corrected depth in medium along the pencil-beam axis, and σ_{MCS} is the root mean square (RMS) of the

lateral spread of the pencil-beam axis due to multiple coulomb scatter at depth z given by the Fermi-Eyges model as follows:

$$\sigma^2_{MCS} = \frac{1}{2}\int_{z_0}^{z}(z-z')^2\frac{d\sigma^2_{MCS}}{dz'}dz'$$

where z' is the coordinate along the pencil-beam axis, z_0 is the coordinate along the pencil-beam at the patient surface, and $d\sigma^2_{MCS}/dz$ is the linear angular scattering power of an electron having the mean energy T.

T is given by Harder's relationship

$$T(z') = T_0\left(1 - \frac{Z_{eff}(z')}{R_p}\right),$$

where T_0 is the initial electron energy, R_p is the practical range, and Z_{eff} is the effective depth given by

$$Z_{eff}(z') = \int_{z_0}^{z}\frac{(dE/dz')}{(dE/dz')_{H_2O}}dz',$$

in which dE/dz' is the linear stopping power at z'.

The first term in equation 16 represents the relative fluence at a calculation point (x, y, z) which is displaced from the pencil-beam axis by $x - x'$ in the x direction and $y - y'$ in the y direction. The second term, $S_{air}(x', y', z)$, represents the fluence on the pencil-beam axis and is given by:

$$S_{air}(x', y', z) = \int_{-\partial field}^{\partial field}\int_{-\partial field}^{\partial field}\frac{1}{2\pi\sigma^2_{air}}\exp\left(-\frac{(x'-x'')^2 + (y'-y'')^2}{2\sigma^2_{air}}\right)dx''dy'', \qquad (17)$$

where σ_{air} is the scatter component due to in-air scatter given by $\sigma_{air} = Z_d\theta_{air}$, in which Z_d is the distance between the sub-beam origin and its endpoint at the calculation depth d and θ_{air} is the mean angular in-air spread of the incident electrons. S_{air} is evaluated over the field projected to the calculation depth z. The remainder of equation 16 performs the fluence-to-dose conversion at the calculation point. (The $-z$ is due to our coordinate convention.)

This pencil beam model does not explicitly model the effect of secondary electron production, so it will not accurately predict the build-up region. In addition, the effect of backscatter caused by electron-electron scatter is ignored. The algorithm attempts to overcome these deficiencies by using measured, broad-beam, depth-dose data to determine the fluence to dose conversion factor.

2.2 Numerical Implementation

Equation 16 is discretized as

$$D(x,y,z) = \sum_{i=0}^{N} \int_{-Wi/2}^{Wi/2}\int_{-Hi/2}^{Hi/2} \frac{S_{air}(x',y',z)}{2\pi\sigma_{MCS}^2} \exp\left(-\frac{(x-x')^2+(y-y')^2}{2\pi\sigma_{MCS}^2}\right) F2D(D_{eff})\frac{SAD+D_{eff}}{SAD-z}dx'dy',$$

where $dx'dy'$ represents the cross-sectional area of the sub-beam having width W and height H and N is the number of sub-beams to be summed. In practice, it is not necessary to add dose contributions from "all" of the sub-beams since the contribution diminishes to a negligible value with increased lateral distance between the calculation point and the sub-beam axis. In the present application, only the contributions from within a lateral distance of $5\sigma_{MCS}$ from the calculation point are considered.

S_{air} must be evaluated over the entire field area. To faciliate the integration, the field is represented in a quadtree format [5] where an irregularly shaped field is subdivided into an optimal number of rectangles. Thus, the integral in equation 17 is replaced by a summation as follows:

$$S_{air}(x',y',z) = \frac{1}{4}\sum_{i=1}^{N}\left(erf\left(\frac{x_i^h - x''}{\sqrt{2}\sigma_{air}}\right) - erf\left(\frac{x_i^l - x''}{\sqrt{2}\sigma_{air}}\right)\right)\left(erf\left(\frac{y_i^h - y''}{\sqrt{2}\sigma_{air}}\right) - erf\left(\frac{y_i^l - y''}{\sqrt{2}\sigma_{air}}\right)\right),$$

where N is the number of rectangles (called "quadtiles") in the quadtree having coordinate (x,y) and upper and lower bounds indicated by the superscripts h and l. The Gaussian integrals in equations 16 and 17 are solved using error functions. In order to increase the computational efficiency the error function values have been pre-computed and stored as a look-up table in a file called `erfvalues`. Execution of the function which looks up the error function values usually comprises approximately half of the computation time required for a dose computation. Consequently, this function has been optimized as much as possible and currently performs only 6 floating point operations.

The current version of the file `erfvalues` contains 59,999 values of the error function for equally-spaced arguments between -6 and 6. The dose computation program sets the error function equal to 0 for arguments ≤ -6 and 1 for arguments ≥ 6. The values contained in `erfvalues` were generated using the utility program `erf.p` which calculates the error function by the polynomial approximation of ACM algorithm 209 [6]. The contents of `erfvalues` are read in and stored in an array by the dose computation program, just prior to reading in the beam data. Subsequently, for arguments in $(-6,6)$, values of the error function are calculated by rounding the argument to the nearest argument for which a value is tabulated and then returning the associated error function value.

σ_{MCS}^2 is evaluated using the recursive relations described by Hogstrom [3]. This allows dose calculations at deeper depths to take some advantage of information calculated for shallower depths but unfortunately only provides a marginal improvement in speed.

The sub-beam transport begins at the cutout plane and is projected onto a calculation plane. The divergence of the sub-beam axis is calculated geometrically using the virtual source position determined by the projection method as described in section 2.3.

The penumbra is determined by the product of two Gaussian spreads, σ_{MCS} and σ_{air}. If necessary, an extra degree of freedom (RMSwt) is allowed to fit the penumbra to the measured data. RMSwt

is a weighting factor for σ_{MCS} which tends to be overestimated at the deeper depth by the Fermi-Eyges theory. RMSwt is a function of depth and is stored in the beam data file for 1 mm increments. If the RMSwt values are not found in the beam data, RMSwt is assumed to be unity.

The fluence-to-dose conversion factor, F2D, is determined from a measured depth-dose curve. This is a depth dependent value and is stored in 1 mm increments to allow for a direct look-up without interpolation.

The dose due to bremsstrahlung is estimated by assuming that the dose beyond the practical range is entirely due to photons as represented by the gamma tail in the measured curve. The photon dose short of the practical range is estimated by linearly back-extrapolating the gamma tail.

Inhomogeneity correction is performed by using the density corrected path length. The organ density must be supplied by the user and should be the ratio of the linear scattering power of the medium to that of water. This value is usually assumed to be energy-independent ([3, p.452]).

Note that the algorithm fails in the physically unrealistic instance where the collimator is inside the patient. This situation will cause the current dose computation program to crash and, therefore, should be avoided.

2.3 Measurements required by the Electron Beam Calculation

1. The incident beam energy (initEnergy) is the "mean energy" determined as per the TG-25 protocol [7, p.86]. It is a function of machine, energy, and applicator size.

2. The practical range R_p is determined from the depth-dose curve according to TG-25 [7, p.85]. It is a function of machine, energy, and applicator size.

3. The virtual source position must be determined by two different methods. The projection method ([7, p.98]) should be used for the determination of the source to collimator distance (SCD) and the inverse square method ([8, p.320ff]) for the virtual source to skin distance (VSSD). Measurements must be obtained for each machine, energy, and applicator size.

4. The mean angular in-air spread of the incident electrons θ_{air} is determined by in-air measurements of the penumbra using film as described in Hogstrom [3, p.454ff]. It is a function of machine, energy, and applicator size. The angular spread is assumed to be isotropic about the beam axis.

5. Depth dose curves vary for each machine, energy, and applicator size. Measurements are taken with an open square field using the standard insert. The curve should include a good portion of the gamma tail. The depth dose curves must be decomposed into the electron and photon components. The photon component is determined from the tail, as described in the previous section. Fluence to dose conversion factors are then calculated by the utility program `f2d.p`.

6. The air profile at or near the cutout plane is measured along the x and y axes of an open square field delineated by the standard insert. Measurements must be obtained for each machine, energy, and applicator size. It is *not* critical that the measurements be taken exactly at the level of the cutout plane.

3 Arc therapy

Dose calculation for an arc field or moving field is performed by computing doses for a series of fixed fields, and summing the results with an appropriate normalization factor. Arc therapy is computed in this same way for photons, electrons and neutrons, using in each case the relevant detailed procedure as already described, for each fixed field step. The first field and the last field in the series are weighted by one-half, relative to each of the other (intermediate) fields. This is essentially a numerical integration over gantry angle, using the trapezoidal rule. If the arc size is less than 50^o, the arc range is divided into ten segments, or eleven fields. If the arc size is 50^o or greater, the number of steps is determined by dividing the arc size by 5 and rounding the result to the nearest whole number. The interval is divided into that number of segments, and the number of fields is then one greater. So, the total number of steps then depends on the angle, but the interval between arc steps is never greater than 5^o.

4 Dose conversion algorithms

In addition to providing facilities to enter, examine, print and plot beam data used in the dose computation, we have implemented two algorithms to convert among different forms of relative central axis dose data and measurements. The two algorithms provide the following operations:

Depth dose to TPR takes photon and neutron beam depth dose measurements and generates tissue-phantom ratios, according to a formula described by Purdy [9].

TPR to SPR takes tissue-phantom ratios and generates tables of modified scatter-phantom ratios, according to equation 11 in Khan [2, pp. 230–237]. Each TPR is multiplied by a ratio of backscatter factors, then the zero-field TPR is subtracted to obtain the scatter component.

The following sections describe these algorithms in more detail.

4.1 Depth Dose to TPR

This procedure takes photon and neutron beam depth dose measurements and generates tissue-phantom ratios, according to the formula in [9].

Purdy's formula is essentially

$$TPR(F_d, D_d) = \frac{DDR(F_{cd}, D_d)}{DDR(F_{cr}, D_r)} \cdot \frac{BSF(F_{cd})}{BSF(F_{cr})} \cdot \left(\frac{SDD}{SDR}\right)^2 \tag{18}$$

However, the definition of depth dose given in section 2 requires that depth-dose always be normalized to 1.0 at the beam's reference depth D_r, *not* the depth of maximum dose, so "ratio of depth doses" simply reduces to the depth dose value at the depth of interest, and the correct field size at that depth.

The procedure works as follows:

1. Prompt user to edit list of backscatter factors. If there is already a list of backscatter factors on file, use it as the starting point. If users want to ignore backscatter factors, they may type in a factor of 1.0 for each field size. In any case, the values that are used are also stored in the beam data record.

2. Calculate TPR's at the same series of depths and almost the same series of field sizes as used in the depth dose table. The field sizes present a problem, because TPR refers to field size at depth and DDR refers to field size at the surface. So, for the smallest field size at which depth dose values are measured, all measurements at depth are actually for larger field sizes. So, most of the TPR's at the smallest field size are actually extrapolated.

4.2 TPR to SPR

This procedure calculates scatter-phantom ratios from tissue-phantom ratios.

The method takes tissue-phantom ratios and generates tables of modified scatter-phantom ratios, according to eqn. 11 in [2]. Each TPR is multiplied by a ratio of backscatter factors, and then zero-field TPR is subtracted to obtain the scatter component.

At each depth d and radius r, the modified SPR is calculated by the formula

$$SPR(r,d) = \left(TPR(r,d) \cdot \frac{BSF(r)}{BSF(0)} \right) - TPR(0,d) \tag{19}$$

where $BSF(0)$ is supposed to be the zero field size backscatter factor. The computation just uses the BSF for the smallest field size in the list, and does not extrapolate. It is permissible of course for the physicist to have entered a value for field size 0.

We use "backscatter factor," in place of what Khan et. al. [2] call "phantom scatter correction factor."

The beam data must already contain a complete tissue phantom ratio table and a table of zero field size TPR's. This procedure generates an SPR table, and also creates the list of depths and radii which are the table indices of the SPR table, and writes them all into the beam data record.

Note that the SPR are calculated directly from the TPR data; we do NOT fit a smooth function to the data, then calculate results using that derived function.

Note also that we calculate plain SPR, not SPR/R. This is different from the convention required by IRREG [**?**], which expected SAR/R.

To obtain SPR from TPR, the following operations are performed:

1. Prompt user to edit list of backscatter factors. If there is already a list of backscatter factors on file, use it as the starting point. If users want to ignore backscatter factors, they can just type in a factor of 1.0 for each field size.

2. The user is prompted to enter the series of radii r at which SPR values will be tabulated. A default list is provided.

3. Field size s (the side of a square) in the TPR table is transformed to radius r for SPR tables, according to the formula $r = s/1.782$ as described in [10, 11]. Interpolation into this modified list is performed to find the TPR's at the series of radii entered by the user. In the same way, the field sizes for backscatter factors are converted to radii and the backscatter factors at the radii specified by the user are derived.

4. The series of depths d at which SPR's are calculated is the same series at which TPR's are tabulated. Thus, no interpolation with respect to depth is performed here.

5. The list of zero-field TPR's found in the beam data are not necessarily at the same series of depths used for SPR's, so they are interpolated to the correct depths.

6. At each depth d and radius r, the modified SPR is calculated by the formula, equation 19.

The procedure actually uses the backscatter factor for the smallest radius in the list. Possibly the user will have estimated the zero fieldsize backscatter factor by extrapolation and entered it into the list. The procedure itself does not perform any extrapolation.

5 Line and point sources

The line source dose calculation uses a table lookup and interpolation method, modified from that of Young and Batho [12]. The attenuation coefficient for the wall of the capsule or needle is taken to be a function of the effective wall thickness rather than a constant.

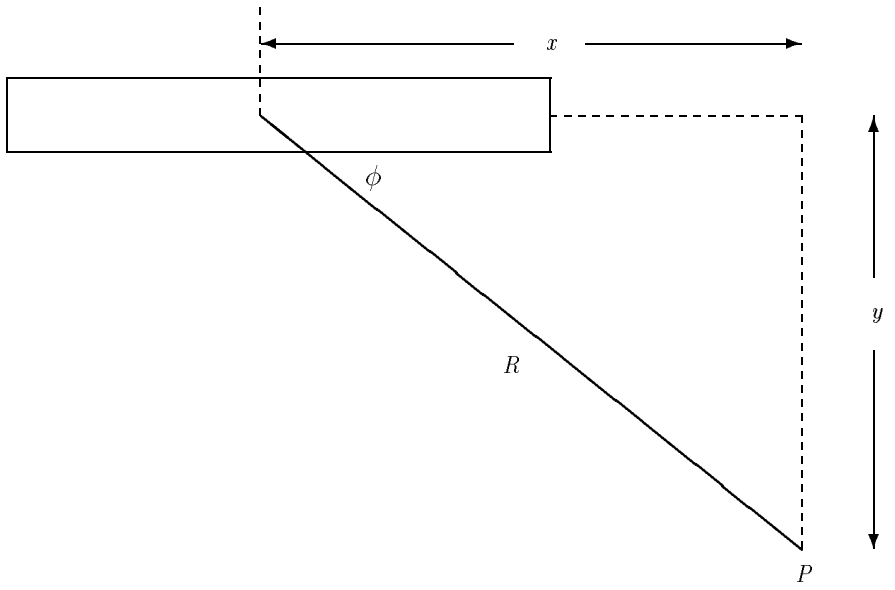

Figure 6: Line source dose computation geometry

The dose at a point whose polar coordinates with respect to the source center are (R, φ) is

$$D = \frac{A\Gamma}{R^2} T(R, \varphi) C(R) \tag{20}$$

where A is the activity or source strength, Γ is the conversion factor between source strength units and absorbed dose units (cGy per source unit), T is an interpolated table factor from a precomputed table and C is a tissue correction factor computed either by a polynomial [13],

$$C = a_0 + a_1 R + a_2 R^2 + a_3 R^3 \tag{21}$$

or by an exponential

$$C = \exp(-\mu_t R) \tag{22}$$

where μ_t is the tissue attenuation coefficient for that source type. See also equation 30 below. The table factor is computed by the Sievert integral method as described in [12], and is generated separately from the radiation treatment planning program dose computation. The tables are generated by using another program, which includes the capability to review and print as well as generate tables for sources of arbitrary filtration. This section describes the modified Sievert integral method used to generate dose factor tables.

This model is not used for point sources. Instead, a simple inverse square formula is used together with the same exponential or polynomial tissue attenuation factor as for line sources,

$$D = \frac{A\Gamma}{R^2} C(R) \tag{23}$$

where C is the tissue correction factor described above.

The line source has active length L and the point P at which we determine the dose rate is at coordinates x, y with respect to a coordinate system in which the x axis is along the source, the y axis is perpendicular to the source, and the origin is at the center of the source. The dose rate at P is obtained by adding up the dose contributions from all the line elements dl,

$$D = \int_{-L/2}^{L/2} \frac{A\Gamma}{r^2} \exp(-\mu d \sec\theta) \frac{dl}{l} \tag{24}$$

which is the Sievert integral. In the above, the quantity d in the exponential is the wall thickness of the line source. Making the usual change of variable from l to θ gives

$$l = x - y \tan\theta \tag{25}$$

$$dl = -y \sec^2\theta d\theta \tag{26}$$

$$r = y \sec\theta \tag{27}$$

so the integral becomes

$$D = \int_{\theta_1}^{\theta_2} \frac{A\Gamma}{y^2 \sec^2\theta} \frac{y \sec^2\theta d\theta}{L} \exp(-\mu d \sec\theta) \tag{28}$$

which becomes

$$D = -\frac{A\Gamma}{yL} \int_{\theta_1}^{\theta_2} \exp(-\mu d \sec\theta) d\theta \tag{29}$$

The location of point P may be more conveniently expressed in the polar coordinates R, φ, where φ is the angle between the source and the line from the source center to point P. Then, since $y = R \sin \varphi$ and the integral may be computed and prestored as a function of θ_1 and θ_2, we may express the dose rate as an inverse square factor times the source strength times a stored table factor.

$$D = \frac{A}{R^2} \left[\frac{R}{L} \frac{\Gamma}{\sin \varphi} S(\theta_1, \theta_2 \right] \tag{30}$$

The limits θ_1 and θ_2 are

$$\theta_1 = \arctan \left[\frac{x - 0.5L}{y} \right] \tag{31}$$

$$\theta_2 = \arctan \left[\frac{x + 0.5L}{y} \right] \tag{32}$$

Note that the quantity in brackets only depends on the so-called "reduced radius" R/L. The quantity in the brackets is computed and stored for a range of values of reduced radius from 0.1 to 6.4, and for a range of values of φ.

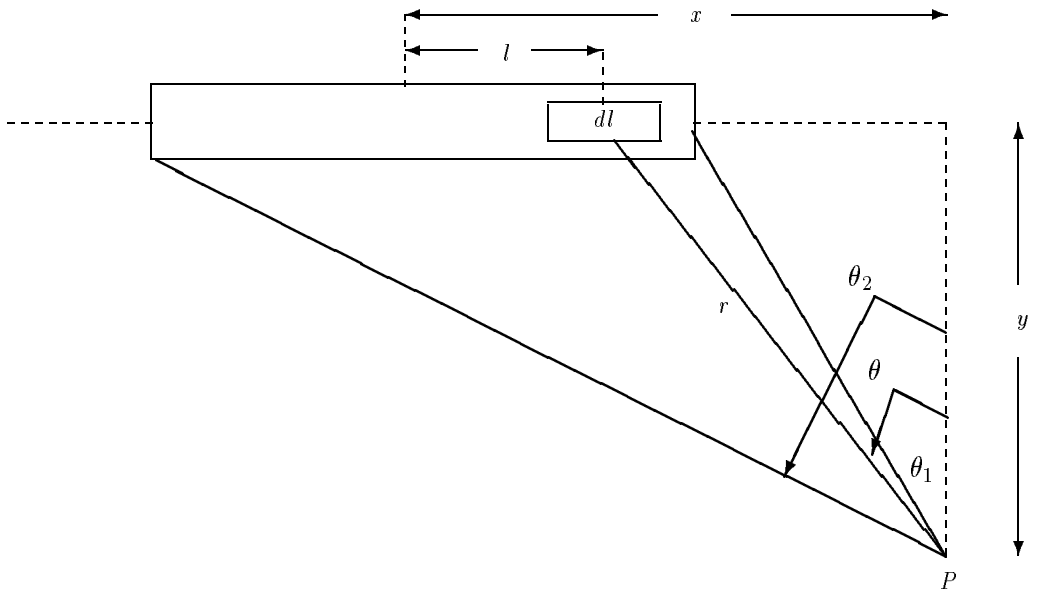

Figure 7: Reference polar coordinates for line sources

For sources such as radium and cesium tubes, the radioactive salt has a finite diameter, giving rise to an effective wall thickness which corresponds to an equivalent line source with an infinitesimally thin radioactive center (the latter is assumed by the Sievert integral method of table generation).

In the calculation of effective thickness, r_s is the radius of the radium (or other) salt, R is the overall radius of the capsule, and t is the nominal wall thickness. Then $R = r_s + t$, and the integral

$$d = \frac{2}{\pi r_s^2} \int_{-r_s}^{r_s} (r_s^2 - r^2)(R^2 - r^2) dr \; - \frac{2.4 r_s}{\pi} \tag{33}$$

gives effective thickness d.

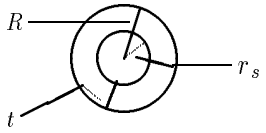

Figure 8: Effective wall thickness

This is exactly as used in the original article by Young and Batho referred to earlier.

If the point P is in line with the source length direction, the Sievert integral is not the means by which to calculate the dose. Instead a different integral is done by the table generation program, which is not independent of active length. However, the Prism system generates a table for each active length so this variation is accounted for.

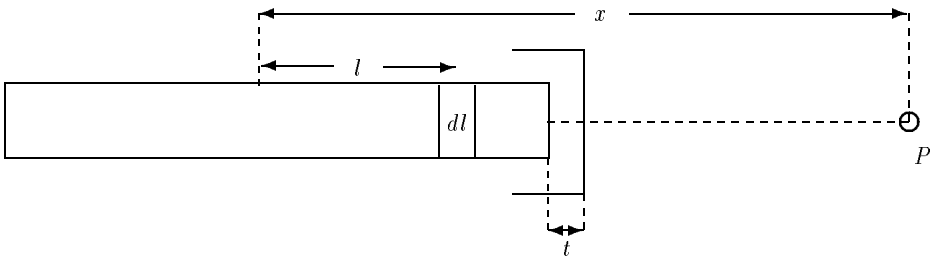

Figure 9: End integral geometry

The integral in this case (points in line with the axis of the capsule) is

$$D = \int_{-L/2}^{L/2} \frac{A\Gamma}{(x-l)^2} \frac{dl}{L} \exp(-\mu t) \exp[-\mu_s (L/2 - l)] \tag{34}$$

which can also be written in terms of the "reduced radius" r for convenience. Let $x = rL$, $l = zL$, so $dl = L\,dz$. Then

$$D = \int_{-0.5}^{0.5} \frac{A\Gamma}{L^2} \exp(-\mu t) \frac{dz}{(r-z)^2} \exp[-\mu_s L(0.5 - z)] \tag{35}$$

which may in turn be written as an activity and inverse square factor times a table factor just as for the off axis values.

$$D = \frac{A}{x^2} T(r) \tag{36}$$

where the table factor $T(r)$ is

$$T(r) = \Gamma r^2 \exp(-\mu t) \int_{-0.5}^{0.5} \frac{dz}{(r-z)^2} \exp[-\mu_s L(0.5 - z)] \tag{37}$$

The quantity μ_s is the self-attenuation of the salt. In the Prism system, it is approximated by using 0.1 times the wall attenuation, both here and in the calculation of the effective radius, above.

References

[1] International Commission on Radiation Units and Measurements. *Determination of Absorbed Dose in a Patient Irradiated by Beams of X or Gamma Rays in Radiotherapy Procedures*. International Commission on Radiation Units and Measurements, Bethesda, MD, 1976.

[2] Faiz Khan, Wilfred Sewchand, Joseph Lee, and Jeffrey Williamson. Revision of tissue-maximum ratio and scatter-maximum ratio concepts for cobalt 60 and higher energy x-ray beams. *Medical Physics*, 7(3):230–237, 1980.

[3] Kenneth R. Hogstrom, Michael D. Mills, and Peter R. Almond. Electron beam dose calculations. *Physics in Medicine and Biology*, 26:445–459, 1981.

[4] L. Eyges. Multiple scattering with energy loss. *Physical Review*, 74:1534–1535, 1948.

[5] Hanne M. Kooy and Peter K. Kijewski. Quadtrees as a representation for irregularly shaped fields in radiotherapy applications. *International Journal of Radiation Oncology, Biology, Physics*, 15:1251–1256, 1988.

[6] D. Ibbetson. *Algorithm 209: GAUSS*, volume 1, pages 209–P 1–3. Association for Computing Machinery, 1980.

[7] American Association of Physicists in Medicine(AAPM). Clinical electron-beam dosimetry: Report of AAPM radiation therapy committee task group no. 25. *Medical Physics*, 18(1):73–109, 1991.

[8] Faiz M. Khan. *The Physics of Radiation Therapy*. Williams and Wilkins, Baltimore, MD, 1984.

[9] James A. Purdy. Relationship between tissue-phantom ratio and percentage depth-dose. *Medical Physics*, 4(1):66–67, 1977.

[10] Bengt Bjarngard and Robert Siddon. A note on equivalent circles, squares, and rectangles. *Medical Physics*, 9(2):258–260, 1982.

[11] M. J. Day. The equivalent field method for axial dose determinations in rectangular fields. *British Journal of Radiology Supplement*, 11:95–100, 1972.

[12] M. E. J. Young and H. F. Batho. Dose tables for linear radium sources calculated by an electronic computer. *British Journal of Radiology*, 37:38–44, 1964.

[13] L. L. Meisberger, R. J. Keller, and R. J. Shalek. The effective attenuation in water of the gamma rays of gold-198, iridium-192, cesium-137, radium-226 and cobalt-60. *Radiology*, 90:953, 1968.